Optics and Laser Technology 94 (2017) 159–164

Contents lists available at ScienceDirect

Optics and Laser Technology

journal homepage: www.elsevier.com/locate/jolt

Full length article

A facetless regrowth-free single mode laser based on MMI couplers

Ludovic Caro [a,b,*], Niall P. Kelly [a,b], Mohamad Dernaika [a,c], Maryam Shayesteh [a], Padraic E. Morrissey [d], Justin K. Alexander [a,b], Frank H. Peters [a,b]

[a] Integrated Photonics Group, Tyndall National Institute, Dyke Parade, Cork, Ireland
[b] Physics Department, University College Cork, College Road, Cork, Ireland
[c] Electrical and Electronic Engineering Department, University College Cork, College Road, Cork, Ireland
[d] Photonics Packaging Group, Tyndall National Institute, Dyke Parade, Cork, Ireland

ARTICLE INFO

Article history:
Received 12 January 2017
Received in revised form 10 March 2017
Accepted 22 March 2017

Keywords:
Semiconductor laser
Single mode
Facetless
Regrowth-free

ABSTRACT

This paper presents a facetless, tunable laser operating near 1575 nm, as well as a theoretical model predicting spectral features of the laser. The lasers were fabricated without regrowth or advanced lithography techniques, and are based on MMI couplers and etched facets. Coarse vernier tuning was achieved over a range of 25 nm, while fine, thermal tuning was also demonstrated over a range of 1.5 nm. SMSR values of 25 dB and higher were observed, with a measured laser linewidth of 600 kHz.

1. Introduction

Single mode, tunable lasers are extensively used in modern communication networks as carrier generators for wavelength division multiplexed (WDM) systems. A common way to achieve single-mode lasing is to use Bragg gratings as in the distributed Bragg reflector (DBR) laser [1], the sampled grating DBR (SGDBR) laser [2], or in the distributed feedback (DFB) laser [3]. However, such lasers require multiple epitaxial growth steps and high-resolution lithography techniques, such as electron beam lithography [4], thus increasing the fabrication time and cost. A regrowth-free alternative is the linear coupling of resonant cavities separated by local defects, such as slots [5]. However, the reflectivity and loss of slots are highly sensitive to the slot width and etch depth, and therefore require careful control of the fabrication process [6]. Regrowth-free DFB lasers have also been reported [7,8] but require holographic lithography to define the gratings, which adds to the fabrication cost.

Another limitation of these lasers is the reliance on cleaved facets as reflectors in the laser's resonant cavity, such as in the Fabry-Perot laser, as well as in more advanced structures such as DBR or SGDBR lasers [9,10]. The use of cleaved facets adds significant constraints to the design of photonic integrated circuits (PICs) by forcing the laser sources to be positioned near a facet of the chip.

This paper presents a regrowth-free, facetless alternative to grating-based lasers, designed to obtain single mode, tunable lasing by combining resonant cavities using etched facets and multimode interference (MMI) couplers [11]. The lasers are fabricated using standard lithography processes and single-step epitaxial growth. While the concept of cavities coupled together through a half-wave coupler has been demonstrated [12], the proposed design also presents an integrated output coupler, making the monolithic integration of other devices with the laser trivial. The design of the laser and its theoretical background are detailed, as well as the fabrication process. The devices are characterized, showing single-mode performance, with both coarse Vernier and fine thermal tunability.

2. Proposed design

The aim of this development is to obtain a single mode, tunable laser that can be placed anywhere on the chip, without requiring advanced lithography techniques or epitaxial regrowth in its fabrication process. Such requirements can be met by coupling multiple resonating cavities of different lengths defined by the spacing between on-chip etched reflectors.

2.1. Coupling cavities to achieve single mode lasing

Single mode lasing can be achieved by coupling two cavities of different lengths, so that only the modes compatible with both

* Corresponding author at: Integrated Photonics Group, Tyndall National Institute, Dyke Parade, Cork, Ireland.
E-mail address: ludovic.caro@tyndall.ie (L. Caro).

http://dx.doi.org/10.1016/j.optlastec.2017.03.029
0030-3992/© 2017 The Authors. Published by Elsevier Ltd.

cavities can lase. The design presented on this paper relies on two cavities coupled through a two-by-two MMI coupler to equally split the input signal from any port, between the two ports at the other end of the coupler. The action of such a coupler is shown in Fig. 1 where the propagation of a signal through the coupler is simulated. The signal is injected into the top-left port, and is equally split between the two right hand side ports.

By coupling two cavities through an MMI coupler, one can ensure that only a limited number of modes are susceptible to lase, thus enabling single mode operation. The MMI serves the additional purpose of providing a single output coupler on one of its output arms, making it possible to collect the laser output and direct it to subsequent photonic devices.

2.2. A facetless design to improve versatility

While the simplest way to obtain reflections and create a resonating cavity for lasers is to use cleaved facets as reflectors, such cleaved facets force the laser sources to be located at the edge of the chip on which the PIC is fabricated, which may be undesirable. On-chip reflectors thus appear as an attractive alternative to facets, allowing the lasers to be positioned away from the chip's edges.

The proposed design uses deeply etched facets to obtain an on-chip reflector. The waveguide end is surrounded by an area etched through the optical confinement region, to obtain a semiconductor/air interface that can be used as a reflector. A gold coating was applied to the end of the waveguide to further improve the facet's reflectivity. Due to the refractive index of gold being lower than 1 around the 1550 nm wavelength [13], a higher reflectivity can be achieved than in the semiconductor/air case. Using the refractive index of Indium Phosphide at 1550 nm [14], one can calculate the reflectivity at normal incidence for both cases: approximately 27% for the InP/air case, and approximately 48% for the InP/Au case. While this calculation is for an ideal case, it shows that applying a gold coating to the etched facet can significantly increase the reflection of the etched facet.

2.3. Achieving vernier and fine thermal tunability

In order to comply with standard WDM communication grids, tunability is necessary to adjust the lasing wavelength to meet the standard carrier wavelengths. To reduce the number of different laser designs involved in a WDM communication system, a single design that reaches a large number of standard wavelengths is desirable. To do so, both wide and fine tuning are necessary. Such properties can be achieved by combining Vernier tuning that allows the lasing wavelength to "jump" to another part of the spectrum, and fine thermal tuning to accurately shift the lasing spectrum to the desired standard wavelength. These two tuning methods make it possible to operate at multiple different wavelengths without changing any design parameters from one laser source to another.

In the proposed design, the two cavities share a common section, which is used for thermal tuning. Each cavity also has a separated independent section for Vernier tuning. The combination of separate and common cavity sections is achieved by using a 2×2 MMI coupler that can split the signal from the common section into the two separate sections of the cavities, and also combine the signal from the two separated sections into the common section. The splitter and combiner functions are illustrated in Fig. 1. The fourth port of the MMI coupler can then be used as an output port to collect the laser light and guide it to the other elements of the PIC.

2.4. Proposed geometry

A two-by-two MMI coupler is used as a central component of the device, and waveguides terminated by gold-coated etched facets are used at three of the coupler's ports. Those three arms form the two cavities of the system, with two independent sections of different lengths for Vernier tuning and one common section for fine thermal tuning. A waveguide is used on the last port to collect the laser signal. It is angled at its termination to minimize any parasitic reflection once it is cleaved for characterization, so that only the cavities defined by the etched facets are affecting the emission spectrum of the laser. A beam propagation simulation was used to optimize the dimensions of the MMI coupler for the 1550 nm wavelength range: 14 μm in width and 290 μm in length. The same beam propagation simulation showed the coupler still achieves its function at a wavelength of 1650 nm. This simulation theoretically confirms the robustness of the MMI coupler against wavelength variations.

Each section of the device can be powered independently, and the electrical isolation is improved by the use of shallow angled slots at their connection points, to increase the electrical isolation while limiting the parasitic reflection thanks to the angle. To

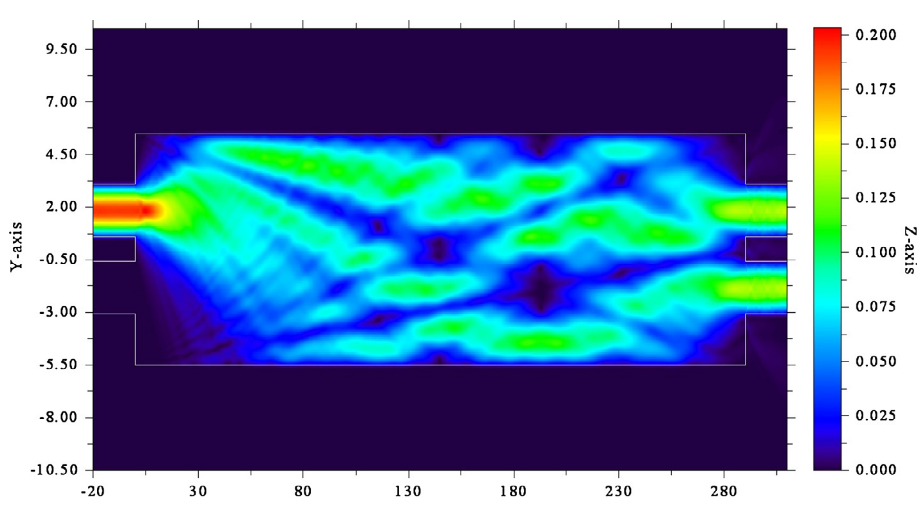

Fig. 1. Simulated signal propagation through a two-by-two MMI coupler at 1550 nm.

further isolate each arm from its neighbor, a deeply (below the quantum wells) etched trench is placed between the adjacent arms, effectively preventing any current leakage from one arm to the other.

The resulting geometry is shown in Fig. 2, for the case where the two cavities have a length difference of 50 μm. The device's total length is approximately 1 mm, and the etched facets allow the device to be positioned anywhere on the chip and to be surrounded by other devices, if required. Metal pads are positioned next to each section, to facilitate probing and injecting current through each section of the laser.

2.5. Theoretical model of the coupled cavities' behavior

A theoretical model of the device's behavior was developed, based on the scattering matrix method (SMM) [15]. Each arm is considered as a two-port system composed of a length of waveguide, terminated by an InP/Au interface. The SMM is used to determine the reflection function of each arm. The reflection functions are then combined through the MMI coupler, to determine the input/output relationship of the device, viewed from the collector arm (labeled 3 in Fig. 2).

In the model, λ is the wavelength of the signal, and $L_k, n_k, g_k(\lambda)$ are the length, refractive index and gain profile of the arm labeled k in Fig. 2. $f_k(\lambda)$ is the reflection function, while $\mathbf{S}_k$ and $\mathbf{T}_k$ are the associated scattering and transmission matrices, corresponding to a waveguide segment terminated by a reflective interface of reflection and transmission coefficients r_k and t_k respectively. The arm is considered as a two-port system: the first port in the propagation direction being the link to the MMI, and the second one being the reflective termination. The desired reflection function is related to the first port, as the behavior of the MMI is studied based on the inputs and outputs at each of its ports. One can write:

$$\mathbf{T}_k = \frac{1}{t_k}\begin{pmatrix} 1 & r_k \\ r_k & 1 \end{pmatrix} \times \begin{pmatrix} \exp(j\phi) & 0 \\ 0 & \exp(-j\phi) \end{pmatrix} \tag{1}$$

$$\mathbf{T}_k = \frac{1}{t_k}\begin{pmatrix} e^{j\phi} & r_k \exp(j\phi) \\ r_k \exp(-j\phi) & \exp(-j\phi) \end{pmatrix}, \tag{2}$$

where $\phi = 2n_k\pi\frac{L_k}{\lambda} + jg_k\lambda L_k$ is the phase shift and amplitude gain induced by the length of the arm. One can thus calculate the scattering matrix for the arm:

$$\mathbf{S}_k = \begin{pmatrix} r_k \exp(-2j\phi) & t_k \exp(-j\phi) \\ t_k \exp(-j\phi) & -r_k \end{pmatrix}, \tag{3}$$

From this equation, it is possible to obtain the reflection function related to the MMI side of the arm. Due to the model chosen for this calculation, the reflection function is the top-left coefficient of the scattering matrix. One can thus write:

$$f_k(\lambda) = r_k \exp(-4jn_k\pi\frac{L_k}{\lambda}) \exp(2g_k\lambda L_k) \tag{4}$$

Once the reflection functions associated to the reflector arms of the structure have been determined, it is possible to study the MMI itself. For this calculation, the MMI is modeled as a waveguide of known length, where any signal entering a port will be equally split between the two opposite ports, with an adequate phase change. In order to reduce the complexity of the calculation, no amplitude variation due to material absorption or gain will be considered.

One can thus use two functions to represent the MMI, one related to the transmission (i.e. from port 1 to port 3), and one related to the coupling (i.e. from port 1 to port 4). Those functions will respectively be called $t(\lambda)$ and $c(\lambda)$, and can be derived from [16] for the 2×2 MMI.

The input and output signals of arm k are labeled i_k and o_k respectively. Note that the terms "input" and "output" are relative to the arm, so that the input is always the signal coming from the MMI, to the arm. The following two sets of equations show these relations:

$$\begin{cases} i_1 = c(\lambda)o_4 + t(\lambda)o_3 \\ i_2 = c(\lambda)o_3 + t(\lambda)o_4 \\ i_3 = c(\lambda)o_2 + t(\lambda)o_1 \\ i_4 = c(\lambda)o_1 + t(\lambda)o_2 \end{cases} \tag{5}$$

$$\begin{cases} o_1 = f_1(\lambda)i_1 \\ o_2 = f_2(\lambda)i_2 \\ o_4 = f_4(\lambda)i_4 \end{cases} \tag{6}$$

The system's full reflection function is defined as $f(\lambda) = \frac{i_3}{o_3}$ with the notation chosen for inputs and outputs. Note that the signal o_3 is not described in (6) because it represents the input signal and as such, is independent from the studied system. Rewriting the expression for i_3:

$$i_3 = c(\lambda)f_2(\lambda)[c(\lambda)o_3 + t(\lambda)o_4] + t(\lambda)f_1(\lambda)[c(\lambda)o_4 + t(\lambda)o_3]. \tag{7}$$

This can be reorganized into the following, replacing o_4 by its expression from (6)

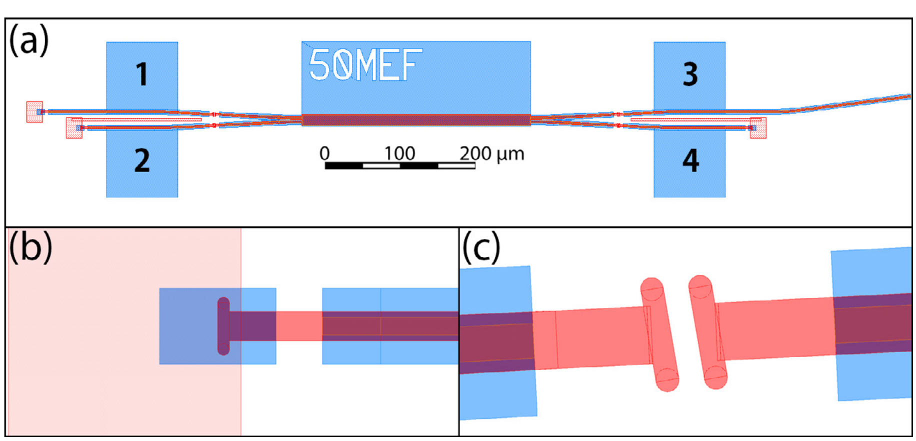

Fig. 2. (a) Schematic of the proposed design with details of (b) a metal-coated deeply etched facet and (c) a shallow electrical isolation slot.

$$i_3 = [c(\lambda)f_2(\lambda)c(\lambda) + t(\lambda)f_1(\lambda)t(\lambda)]o_3 + [c(\lambda)f_2(\lambda)t(\lambda) + t(\lambda)f_1(\lambda)c(\lambda)]f_4(\lambda)i_4. \quad (8)$$

Following a similar procedure, i_4 can be expressed as a function of o_3:

$$i_4 = [c(\lambda)f_1(\lambda)t(\lambda) + t(\lambda)f_2(\lambda)c(\lambda)]o_3 + [c(\lambda)f_1(\lambda)c(\lambda) + t(\lambda)f_2(\lambda)t(\lambda)]f_4(\lambda)i_4$$
$$i_4 = o_3\frac{[c(\lambda)f_1(\lambda)t(\lambda) + t(\lambda)f_2(\lambda)c(\lambda)]}{1 - [c(\lambda)f_1(\lambda)c(\lambda) + t(\lambda)f_2(\lambda)t(\lambda)]f_4(\lambda)}. \quad (9)$$

Using (9) in (8), one can conclude for the system's reflection function $f(\lambda) = \frac{i_3}{o_3}$:

$$f(\lambda) = c(\lambda)f_2(\lambda)c(\lambda) + t(\lambda)f_1(\lambda)t(\lambda) + [c(\lambda)f_1(\lambda)t(\lambda) + t(\lambda)f_2(\lambda)c(\lambda)] \times \frac{[c(\lambda)f_2(\lambda)t(\lambda) + t(\lambda)f_1(\lambda)c(\lambda)]}{1 - [c(\lambda)f_1(\lambda)c(\lambda) + t(\lambda)f_2(\lambda)t(\lambda)]f_4(\lambda)}. \quad (10)$$

This equation is the reflection function of the 2×2 MMI coupled cavity structure, and can be used to predict some elements of the laser's behavior, such as the mode and super-mode spacing. An example of simulated reflection profile is shown in Fig. 3 for the case of a laser device with 50 µm of cavity length difference.

3. Fabrication process

The devices were fabricated from commercial 1550 nm laser material grown on an InP substrate. The active region included 5 compressively strained quantum wells based on AlInGaAs, with a total thickness of 0.4 µm. The wafers were processed using a combination of silicon oxide and silicon nitride layers as hard masks to obtain two different self aligned etch depths. One etch level is immediately above the quantum wells to define standard waveguide and MMI structures, and the other level is deeper than the quantum wells, where reflective structures such as etched facets are needed. Only standard UV lithography was used during the fabrication process, with an alignment resolution of approximately 1 µm. The metal contacts were patterned using standard lift-off lithography, and were based on Ti:Au (20:250 nm) deposited by electron-beam evaporation. A 360° rotational tool was used to ensure continuous metal deposition on the side walls, to avoid breaks causing open circuits and to obtain adequate gold deposition on the etched facets. More details on similar fabrication processes can be found in [17,18].

After processing, the wafers were cleaved to separate the devices. An example of those presented in this paper are shown in Fig. 4, along with other devices fabricated during the same process. A scanning electron microscope (SEM) picture details an etched facet, showing the deeply etched region and the metal coating. The T-shaped termination of the etched facet is used to ensure the facet is flat by pushing the corners farther away from the reflection area. By doing so, the imperfect resolution of the lithography has a limited impact on the quality of the reflective facet.

4. Characterization results

After cleaving, each section was biased independently, by applying currents ranging from 0 to 50 mA for the reflector arms, and up to 180 mA for the MMI coupler. In order to prevent any damage to the devices, the bias voltages were maintained below 2.5 V. The emitted light was collected by a lensed fiber coupled to the output waveguide of the device. The devices were stabilised at a temperature of 20 °C by the means of a Peltier cooler that maintained the temperature of the chuck on which the devices were placed.

4.1. Lasing characterisation

Lasing was successfully achieved at a variety of wavelengths for each device, across a 25 nm wavelength range. Lasing powers of up to −10 dBm were coupled into the collector fiber, as shown in Fig. 5(a). The linewidth was measured using a standard self-heterodyne technique using 50 km of fibre. The lasers presented here were measured to have a linewidth of 600 kHz, which is half of the full width at half maximum of the self-interference profile shown in Fig. 5(b).

In order to confirm that only the cavities defined by the etched facets were lasing, a Fourier analysis of the emission spectra below threshold was performed. The Fourier analysis, showed in Fig. 6 for the 100 µm cavity length difference case, allowed to determine the lengths of the cavities leading to the spectrum observed. The two main cavity lengths can clearly be observed near the 900 µm and 1000 µm length, as well as the peak at 100 µm corresponding to the super-mode spacing. The absence of a peak at 290 µm (length of the coupler) shows that no significant reflection occurs at the ends of the MMI coupler. This can indicate that the laser input is successfully directed to the output ports, confirming the coupler dimensions are adequate to achieve its function in the emission wavelength range.

4.2. Tuning performance

Various bias configurations were studied for this laser. By changing the bias of one or both of the sections of different lengths (on the left side on the schematic and SEM pictures), it was possible to obtain lasing at wavelengths corresponding to each super-mode, over a span of approximately 25 nm, as illustrated in Fig. 7. At each of the lasing wavelengths, a side mode suppression ratio (SMSR) equal or higher to 25 dB was achieved. The currents used to obtain those lasing spectra were typically in the 10–50 mA range for the arms and 70–100 mA for the MMI coupler.

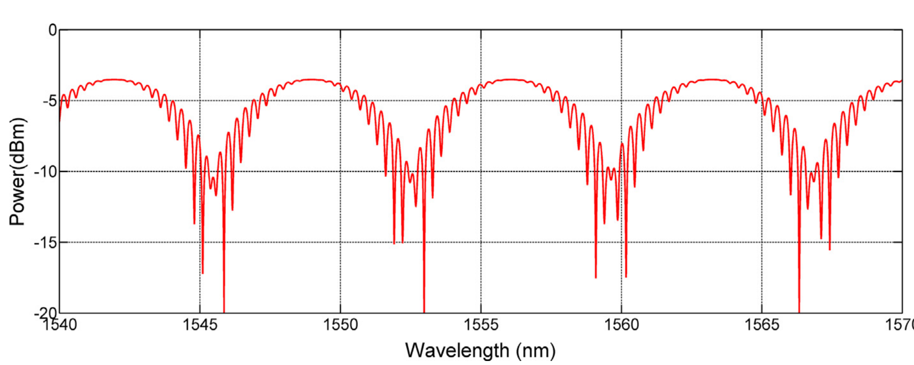

Fig. 3. Simulated reflection profile of a device with a 50 µm cavity length difference.

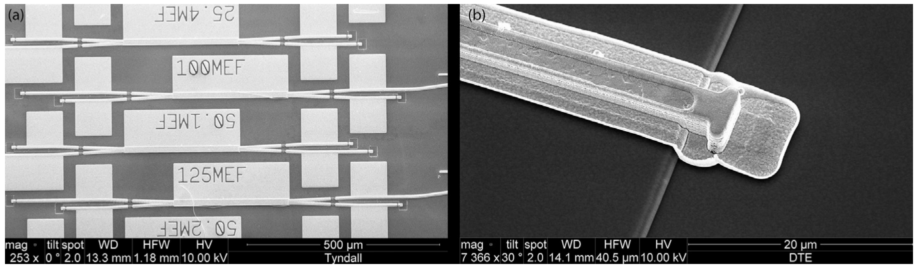

Fig. 4. SEM images of (a) the completed devices and (b) an etched facet.

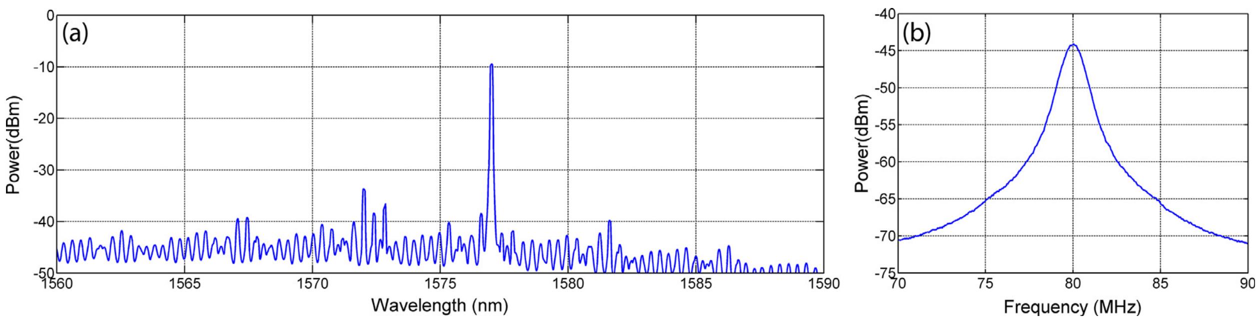

Fig. 5. Laser (a) emission spectrum and (b) self-interference profile with a 75 µm cavity length difference.

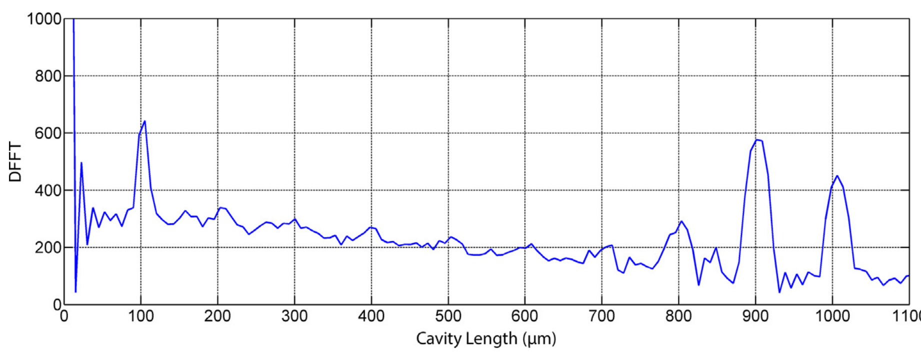

Fig. 6. Fourier analysis of a laser emission spectrum with a 100 µm cavity length difference.

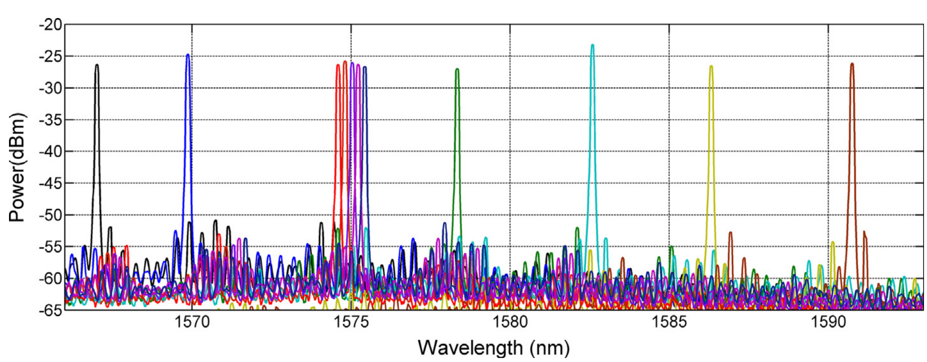

Fig. 7. Vernier tuning and thermal adjustment of the laser with a 100 µm cavity length difference.

Adjusting the bias of the common sections (MMI or common reflective arm) enabled fine tuning of the lasing wavelength. A tuning span of approximately 1.5 nm was achieved, as shown in Fig. 7 with an illustration of fine tuning around the 1575 nm wavelength.

The proposed laser thus achieved both Vernier and fine thermal tuning, reaching a number of wavelengths while maintaining the SMSR above 25 dB.

4.3. Comparison with the theoretical model

The spectra collected during the characterization process were compared to the reflection profiles predicted by the simulation presented above, where the theoretical curves were adjusted in the absolute location of wavelength to best match the experimental data. The mode and super-mode spacing values predicted by

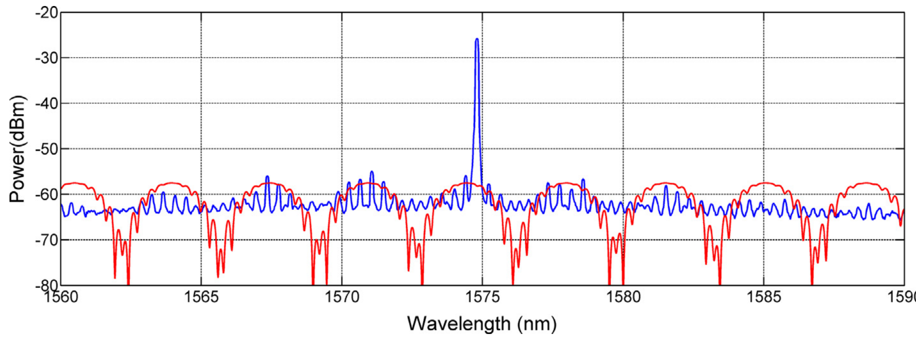

Fig. 8. Emission spectrum of a laser (blue) compared with the system's simulated reflection profile (red, not to scale). (For interpretation of the references to colour in this figure legend, the reader is referred to the web version of this article.)

the model showed good agreement with the emission spectra, as shown in Fig. 8.

The simulation model, although lacking accuracy to predict the exact position of the super-modes, proved to be effective as a means to predict the super-mode and mode spacing of the proposed coupled cavity laser. The knowledge of such characteristics can prove useful to predict the adequate laser dimensions in systems requiring multiple wavelengths, in order to design and fabricate a laser able to reach as many wavelengths as possible.

5. Conclusion

A tunable, single mode laser based on MMI couplers and on-chip etched facets was demonstrated. A theoretical model was developed, predicting features of the laser such as mode and super-mode spacing. The lasers were fabricated using a regrowth-free process based on standard lithography and etch techniques. The characterization of the devices showed both Vernier and fine thermal tunability, with SMSR values equal to or higher than 25 dB and a linewidth of 600 kHz. The lasing spectra showed good agreement with the theoretical model, regarding mode and super-mode spacing. Those devices represent an alternative to grating-based lasers that does not require costly and time-consuming processes such as regrowth or advanced lithography techniques, making them attractive for production at large scales.

Acknowledgment

This work was supported by the Science Foundation Ireland under grants SFI 10/CE/I1853 (CTVR2) and SFI 13/IA/1960.

References

[1] W. Tsang, R. Logan, L. Johnson, R. Hartman, L. Koszi, Strip buried heterostructure lasers with passive distributed Bragg reflectors, IEEE J. Quant. Electron. 15 (1979) 1091–1093.

[2] V. Jayaraman, Z.-M. Chuang, L. Coldren, Theory, design, and performance of extended tuning range semiconductor lasers with sampled gratings, IEEE J. Quant. Electron. 29 (1993) 1824–1834.

[3] S. Chinn, Effects of mirror reflectivity in a distributed-feedback laser, IEEE J. Quant. Electron. 9 (1973) 574–580.

[4] J. Buus, M. Amann, D. Blumenthal, Tunable Laser Diodes and Related Optical Sources, Wiley-IEEE Press, 2005.

[5] B. Corbett, C. Percival, P. Lambkin, Multiwavelength array of single-frequency stabilized Fabry-Perot lasers, IEEE J. Quant. Electron. 41 (2005) 490–494.

[6] S. O'Brien, E.P. O'Reilly, Theory of improved spectral purity in index patterned Fabry-Perot lasers, Appl. Phys. Lett. 86 (2005).

[7] J. Wang, J.-B. Tian, P.-F. Cai, B. Xiong, C.-Z. Sun, Y. Luo, 1.55 – µm algainas-inp laterally coupled distributed feedback laser, IEEE Photon. Technol. Lett. 17 (2005) 1372–1374.

[8] S.J. Jang, C.I. Yeo, J.S. Yu, Y.T. Lee, 1.55 – μm dfb lasers with narrow ridge stripe and second-order metal surface gratings by holographic lithography, Phys. Stat. Solidi (a) 207 (2010) 1982–1987.

[9] J. Johnson, L.-P. Ketelsen, D. Ackerman, L. Zhang, M. Hybertsen, K. Glogovsky, C. Lentz, W. Asous, C. Reynolds, J. Geary, K. Kamath, C. Ebert, M. Park, G. Przybylek, R. Leibenguth, S. Broutin, J. Stayt, J.W., K. Dreyer, L. Peticolas, R. Hartman, T. Koch, Fully stabilized electroabsorption-modulated tunable dbr laser transmitter for long-haul optical communications, IEEE J. Select. Top. Quant. Electron. 7 (2001) 168–177.

[10] C.-L. Yao, S.-L. Lee, I.-F. Jang, W.-J. Ho, Wavelength-selectable lasers with Bragg-wavelength-detuned sampled grating reflectors, J. Lightwave Technol. 24 (2006) 3480–3489.

[11] L. Soldano, E. Pennings, Optical multi-mode interference devices based on self-imaging: principles and applications, J. Lightwave Technol. 13 (1995) 615–627.

[12] J. Jin, L. Wang, T. Yu, Y. Wang, J.-J. He, Widely wavelength switchable v-coupled-cavity semiconductor laser with ~40 dB side-mode suppression ratio, Opt. Lett. 36 (2011) 4230–4232.

[13] A.D. Rakić, A.B. Djurišić, J.M. Elazar, M.L. Majewski, Optical properties of metallic films for vertical-cavity optoelectronic devices, Appl. Opt. 37 (1998) 5271–5283.

[14] G.D. Pettit, W.J. Turner, Refractive index of InP, J. Appl. Phys. 36 (1965) (2081-2081).

[15] L.A. Coldren, S.W. Corzine, M.L. Mašanović, Diode Lasers and Photonic Integrated Circuits, John Wiley & Sons, Inc., 2012.

[16] K. Cooney, F.H. Peters, Analysis of multimode interferometers, Opt. Exp. 24 (2016) 22481–22515.

[17] P.E. Morrissey, N. Kelly, M. Dernaika, L. Caro, H. Yang, F.H. Peters, Coupled cavity single-mode laser based on regrowth-free integrated MMI reflectors, IEEE Photon. Technol. Lett. 28 (2016) 1313–1316.

[18] H. Yang, P. Morrissey, W. Cotter, C.L.M. Daunt, J. O'Callaghan, B. Roycroft, N. Ye, N. Kelly, B. Corbett, F.H. Peters, Monolithic integration of single facet slotted laser, SOA, and MMI coupler, IEEE Photon. Technol. Lett. 25 (2013) 257–260.